Twilight sky brightness measurements as a useful tool for stratospheric aerosol investigations

Nina Mateshvili,[1] Didier Fussen,[2] Filip Vanhellemont,[2] Christine Bingen,[2] Erkki Kyrölä,[3] Iuri Mateshvili,[1] and Giuli Mateshvili[1]

Received 13 October 2004; revised 3 February 2005; accepted 8 March 2005; published 13 May 2005.

[1] In this paper we demonstrate how twilight sky brightness measurements can be used to obtain information about stratospheric aerosols. Beside this, the measurements of the distribution and the variability of the twilight sky brightness may help to understand how the stratospheric aerosols affect the radiation field, which is important for correct calculations of photodissociation rates. Multispectral measurements of twilight sky brightness were carried out in Abastumani Observatory (41.8°N, 42.8°E), Georgia, South Caucasus, during the period (1991–1993) when the level of stratospheric aerosols was substantially enhanced after the 1991 Mount Pinatubo eruption. The twilight sky brightness was measured at 9 wavelengths (422, 474, 496, 542, 610, 642, 678, 713, and 820 nm) for solar zenith angles from 89° to 107°. There are clear indications of a growth of the stratospheric aerosol layer after the eruption of Mount Pinatubo that manifests itself by "humps" in twilight sky brightness dependences versus solar zenith angle. Similar features were obtained using a radiative transfer code constrained by the SAGE II aerosol optical thicknesses. It is shown how an enhancement of stratospheric aerosol loading perturbs the twilight sky brightness due to light scattering and absorption in the aerosol layer. The influence of ozone variations and background stratospheric aerosols on twilight sky brightness has also been analyzed. The optical thicknesses of the stratospheric aerosol layer obtained from the twilight measurements of 1990–1993 show a good agreement with SAGE II results. The spectral variations of the stratospheric aerosol extinction for pre-Pinatubo and post-Pinatubo measurements reflect the aerosol growth after the eruption. Finally, the utilization of twilight sky brightness measurements for validation of satellite-based measurements of the stratospheric aerosol is proposed.

Citation: Mateshvili, N., D. Fussen, F. Vanhellemont, C. Bingen, E. Kyrölä, I. Mateshvili, and G. Mateshvili (2005), Twilight sky brightness measurements as a useful tool for stratospheric aerosol investigations, *J. Geophys. Res.*, *110*, D09209, doi:10.1029/2004JD005512.

1. Introduction

[2] Investigations of the stratospheric aerosols are important for a better understanding of their possible influence on climate, because of their role in atmospheric chemistry, radiative forcing and by considering them as atmospheric dynamics tracers. The long-term satellite-borne atmospheric experiments of the last two decades have yielded global-scale data about many atmospheric constituents including stratospheric aerosols. But, to provide a complete and reliable estimate of the properties of stratospheric aerosols, it is desirable to validate satellite data with other methods, i.e. in situ sampling and remote scattering measurements [*Ackerman et al.*, 1989]. Spectral measurements of twilight sky brightness in visual diapason may serve as one of such supplementary measurements.

[3] The idea of using the twilight phenomenon for an investigation of the atmospheric aerosols has a long history. A bright purple color of twilight after the Krakatau eruption in 1883 allowed to suggest the presence of an aerosol layer in the stratosphere. Several investigators used photometrical measurements of the twilight sky at one or more wavelengths to detect stratospheric aerosol enhancements after strong volcanic eruptions [e.g., *Volz*, 1975; *Volz and Goody*, 1962; *Shakh*, 1969; *Mateshvili et al.*, 1998; *Mateshvili and Rietmeijer*, 2002]. But a lack of theoretical investigations did not allow to obtain quantitative parameters of the stratospheric aerosol layer (referred to as SAL hereafter), such as aerosol extinction profiles.

[4] On the other hand, measurements of distribution and variability of twilight sky brightness may help to understand how aerosols affect the radiation field, which is important for correct calculations of photodissociation rates. *Anderson et al.* [1995] has shown that in case of a strong volcanic eruption, optical effects of aerosols may cause a major

[1] Abastumani Astrophysical Observatory, Tbilisi, Georgia, South Caucasus.
[2] Belgian Institute for Space Aeronomy, Brussels, Belgium.
[3] Finnish Meteorological Institute, Helsinki, Finland.

0148-0227/05/2004JD005512

perturbation in photochemistry at twilight, especially in polar regions.

[5] The June 1991 eruption of Mount Pinatubo caused a dramatic increase of aerosol loading in the stratosphere. The injected material has produced numerous important effects on the atmosphere [*Russell et al.*, 1996, and references therein] such as atmospheric warmings and coolings, a decrease in the net radiative flux at the top of the atmosphere, ozone depletions due to heterogeneous reactions on the aerosol surface. The variations of stratospheric aerosol loading were extensively investigated by means of different remote sensing techniques, such as global satellite monitoring, lidar, sunphotometer, and in situ measurements by optical counters and stratospheric dust samplers.

[6] The goal of this article is to demonstrate how measurements of twilight sky brightness can serve for investigations of the stratospheric aerosols by analyzing which aerosol parameters can be retrieved from the measurements and how variations of the stratospheric aerosol loading can redistribute brightness of the twilight sky.

[7] For this purpose we consider the measurements of twilight sky brightness carried out in Abastumani Astrophysical Observatory, Georgia, South Caucasus, that covered the Pinatubo eruption in June1991.

2. Experimental Technique

[8] In this section we describe schematically the experimental set-up used for the observation of the twilight brightness variation [e.g., *Mateshvili et al.*, 1998]. When the Sun is below the horizon, i.e. when solar zenith angle (SZA) is greater then 90° (Figure 1, points B and C), the lower part of the atmosphere is obscured by the Earth's shadow while its upper part is illuminated. The boundary between the illuminated and shadowed parts (ray SC_1, Figure 1) is monotonously shifting up with the increase of SZA. The twilight sky brightness at any given moment is caused by the total light that is scattered towards an observer (consecutively located in points A, B, C, Figure 1) from all air molecules and aerosol particles above this boundary. For a moderate stratospheric aerosol loading the main contribution to the twilight brightness is given by the lowest and therefore densest sunlit layer. The light scattered in the atmosphere above the lower sunlit layer can be neglected due to the rapid decrease of the atmospheric density with increasing altitude. *Rozenberg* [1966] developed a theory of the twilight in case of a moderate aerosol loading. It allowed to estimate the altitude of a particular scattering atmospheric layer at each value of SZA. An analysis of light intensities scattered at different altitudes allowed to detect the presence of aerosol at these altitudes [*Mateshvili et al.*, 1998; *Mateshvili and Rietmeijer*, 2002]. A quite different situation takes place in presence of high aerosol loading. In this case the SAL, while sunlit, adds significantly to sky brightness in comparison with Rayleigh scattering by air just above the boundary of the Earth's shadow. The SAL significantly disturbs the twilight sky brightness and the simple idea that the lowest sunlit layer at every given moment gives the main contribution to the light scattered towards the observer is no longer correct, making it impossible to estimate the properties of the layer by using the classical theory of twilight.

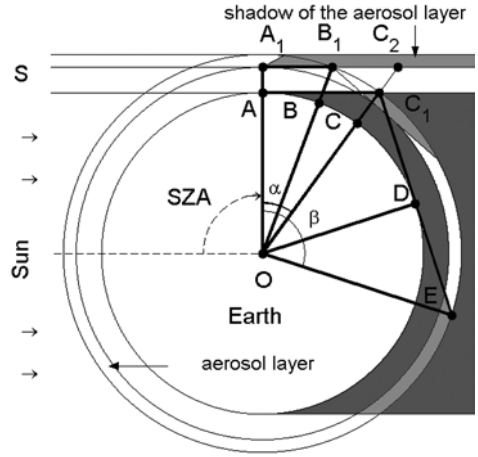

Figure 1. The scheme of the twilight event. The photometer is pointed to the zenith and passes consecutively points A, B, C as the Earth rotates during twilight. The dashed arc indicates the solar zenith angle SZA for an observer located in the point A. The Earth and the stratospheric aerosol layer cast shadows on the atmosphere.

[9] Even in case of moderate aerosol loading, the Rozenberg theory does not allow to obtain important aerosol characteristics as the mean radius and the approximate size distribution. This opportunity appeared only when elaborated radiative transfer models had been developed.

[10] The twilight sky brightness measurements were carried out in Abastumani Observatory (41.8°N, 42.8°E) by means of a photometer with 9 spectral channels. The measurements were carried out in three directions: one with zenith distance 0° and two with zenith distance 60°. The last two differed by their azimuth: one had the same azimuth as the Sun and the azimuth of another was 180° greater. Photomultipliers working in photon-counting mode were used as light receivers. The photometer was equipped with interference filters centered at λ = 422, 474, 496, 542, 610, 642, 678, 713 and 820 nm, with half-width $\Delta\lambda \approx 5$ nm. Fields of view of the optical channels corresponded to an angular diameter equal to 1°. The experimental data were obtained in arbitrary units.

[11] The dynamical range of the available light receiver was not sufficient to cover day-to-night variation of the sky brightness. Sets of attenuators were used to keep the signals within the sensitivity range of the receivers. As a result, an entire twilight curve was presented by a few fragments with different attenuation factors. The following procedure was used for its reconstruction. The fragments were plotted on logarithmic scale. The ends of the segments were linearly extrapolated using the least square method. The factors of attenuation for each pair of segments were calculated and the segments were respectively renormalized. Thus, the measurements themselves served as a periodic calibration procedure. It gave an opportunity to consider currently occurring conditions, such as spectral distributions and apertures of the incident light beams, and also a possible ageing of attenuators.

[12] The measurements were carried out during the 1989–1993 period. This period included the major volcanic eruption of Pinatubo in June 1991, the preeruption strato-

spheric aerosol situation and also the posteruption decay of the Pinatubo aerosol.

3. Observations

[13] In this section we describe our experimental results and discuss the possible reasons of variations of twilight sky brightness basing ourselves on a simple geometry. For this purpose we also model horizontal transparency of the atmosphere in presence of an enhanced SAL and consider the light scattered by the SAL towards the observer.

[14] Figure 2 represents the logarithmic twilight sky brightnesses in arbitrary units as a function of SZA (called ''twilight curves'' hereafter) for pre-Pinatubo (dotted line) and post-Pinatubo (solid line) cases. The twilight curves were measured at viewing zenith angle (VZA) $z = 60°$ and with the same value of azimuth as the Sun actually had. The SZAs are calculated from local time at each measurement point. The procedure of time to SZA convertion is described in many astronomical handbooks [e.g., *Montenbruck and Peleger*, 2000]. In case of morning twilight SZA decreases in course of time while in case of evening twilight SZA increases.

[15] The pre-Pinatubo curve shows a monotonous decrease as SZA increases. The light intensity decreases rapidly at SZA's greater than 90° until it reaches a plateau corresponding to nightglow background. The shape of the post-Pinatubo curve is quite different. It shows a prominent hump (I) in the range of SZA's 92–94° and a less prominent one (II) in the range 98–100°.

[16] The humps on twilight curves in SZA range 92–94° were also reported by *Ashok et al.* [1982, 1984] and *Chakrabarty and Lal* [1997], after strong volcanic eruptions such as El-Chichon and Pinatubo. The hump I is likely to be related with the phenomenon of purple light which consists in the reddening of a western segment of the sky at 92–94° of SZA. The hump II may be connected with the phenomenon of the so-called ''second purple light'' that was observed after the eruption of Krakatau in August 1883 [*Deacon*, 1956]. The phenomenon of the second purple light resembles in general features the phenomenon of the first purple light, although it occurs at larger SZA. *Gann* [1902] reported that both first and second purple lights, exceptionally bright and durable, were observed during the late fall and winter 1883–1884.

[17] Let us consider physical reasons of the hump I appearance on twilight curves. Figure 1 shows a simplified representation of the twilight event in the presence of a strong SAL shown by a ring. We consider how the twilight light intensity changes with the increase of SZA for measurements in the zenith direction. For each SZA value only particular sun rays are able to reach the currently observed volume of SAL and to be scattered by it in the viewing direction. When SZA becomes larger than 90°, the sun rays (SB_1) pass the longest way in SAL and are heavily attenuated causing a rapid decrease of the twilight sky brightness. The SAL even casts a shadow on the upper stratosphere. With further increase of SZA, the sun rays (SC_1) cross the SAL, then pass under it to cross the SAL again. They are less attenuated and are successfully scattered by aerosol towards the observer (C_1C) making a contribution to the measured twilight sky brightness and

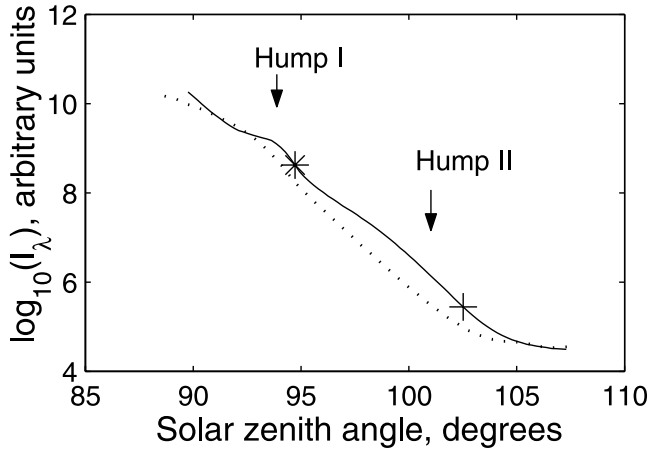

Figure 2. Logarithms of twilight sky brightnesses versus solar zenith angle for background (dashed line, February 5, 1989, morning) and volcanic (solid line, November 16, 1991, morning) conditions. The wavelength of measurements is 713 nm. The viewing zenith angle is 60°. The viewing azimuth coincides with the solar azimuth. Asterisk and cross mark the points of maximal rates of decay.

slowing the decrease of the twilight curve (hump I, Figure 2). When the SAL enters the shadow of the Earth, the layer does not contribute any more to the scattered light but only attenuates the light scattered in the upper layers of the atmosphere towards the observer. As a result, the twilight light intensity decreases rapidly. We can conclude that the hump I appears due to the favorable conditions of the SAL illumination in some range of SZA. A rather similar explanation of the origin of the humps on twilight curves was presented by *Ashok et al.* [1982].

[18] Considering the right triangles OA_1B_1 and OAC_1 we can easily estimate SZA's (AOB + $\pi/2$ and AOC + $\pi/2$) between which the hump on the twilight curve must be expected. Such a crude estimate may be helpful as a starting guess for the retrieval of the aerosol extinction profile.

[19] To illustrate the simple explanation presented above we have made calculations of the horizontal transmittance versus altitude for three values of SZA (90°, 92°and 94°) and the wavelength $\lambda = 700$ nm in presence of the Pinatubo aerosol (Figure 3). The used aerosol extinction profile is represented on Figure 4 by a solid line. The same profile was also used to fit twilight measurements of Nov. 8, 1991 (see Figure 11 below). Only primary scattering was considered. The attenuation in the SAL manifests itself as minima (marked by crosses) on the transmittance curves. We see on Figure 3 that the altitude of minimum increases with the increase of SZA. Let us consider Figure 1 to understand this effect. Lines AA_1, BB_1 and CC_2 represent the altitudes of the SAL's shadow for different SZAs. We see that with the increase of SZA the altitude also increases. At SZA = 94° (Figure 3) the maximum of transmittance is at the SAL's altitude, the minimum is just above the SAL and the troposphere is shadowed by the Earth.

[20] Let us consider the light scattered by the SAL towards the observer. The growth of the posteruption aerosol particles leads to a prevalence of light scattered forward. But in case of considered ground-based observations we register the light scattered sidewards. We can

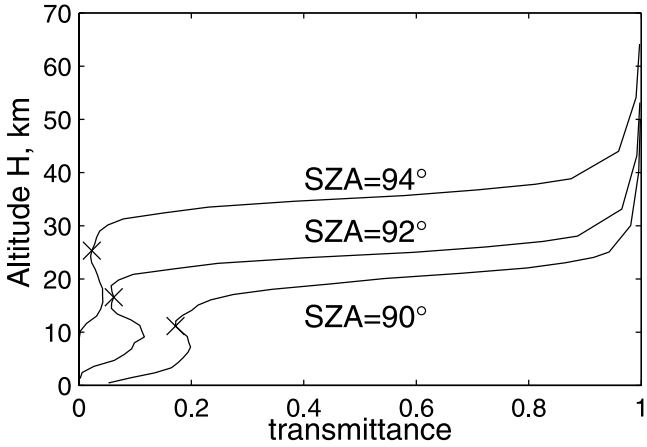

Figure 3. Horizontal transmittance dependence from altitude for different values of the solar zenith angle (SZA) in the presence of the stratospheric aerosol layer. Crosses mark the minima of transmittance caused by the attenuation in the layer. The aerosol extinction profile used in this calculation is shown by solid line on Figure 4. The wavelength of modeling is 700 nm.

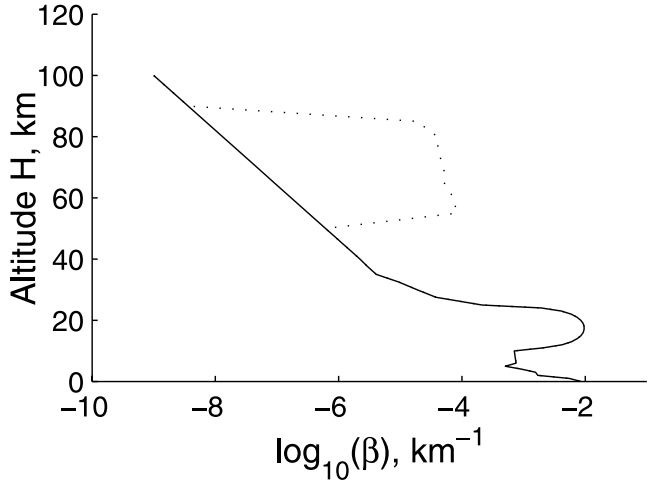

Figure 4. The aerosol extinction profile (solid line). This profile was used for modeling of transmittance presented on Figure 3 and twilight curves presented on Figure 11. The mesospheric aerosol layer is indicated by dotted line. This addition will be discussed in chapter 7.

detect this light if its intensity exceeds the Rayleigh scattering in the same direction. Figure 5 shows aerosol and Rayleigh angular scattering calculated for 700 nm (solid line) and 400 nm (dotted line). The goal of the presented calculation is to show that a real size distribution, which was measured in-situ, can produce a detectable change in the twilight sky brightness. The aerosol angular scattering was calculated using the Mie theory and the in-situ post-Pinatubo aerosol size distribution obtained from an airborne dust collection [*Pueschel et al.*, 1994]. The data were averaged over three measurements attributed to Nov. 2, 1991. The latitudes of the three in-situ measurements (41; 41; 43°N) are close to the latitude of our observational place (41.8°N). Although the longitude of the in-situ measurements (74; 90; 107°W) and the longitude of our measurements (42.8°E) are essentially different, we consider that the size distribution is quite suitable for our purpose.

[21] The refractive index 1.45 was used, which is the representative value for the considered wavelengths 400 nm and 700 nm [*Russell et al.*, 1996]. We made the calculation of the Rayleigh angular scattering for the altitude of aerosol collection at 19 km. We see that for VZA = 0° the sidewards aerosol scattering value (marked by asterisk in Figure 5) approximately equals to the Rayeigh scattering at 700 nm and is smaller than Rayleigh scattering at 400 nm. For measurements with VZA = 60° and in the solar azimuth (cross in Figure 5) aerosol scattering exceeds the Rayleigh scattering for the wavelength 700 nm and equals to the Rayleigh scattering for the wavelength 400 nm. And, indeed, we see that we have the most prominent "hump" on the twilight curve obtained at the longest wavelength of the measurements (Figure 6).

4. Radiative Transfer Model

[22] In order to obtain quantitative characteristics about the SAL it is necessary to use a radiative transfer (RT) model. In this chapter we discuss the used RT model, its input parameters and the approximations used in it. The main difficulty of the twilight sky brightness analysis is that a plain parallel approximation of the atmosphere is not valid in twilight conditions.

[23] A freely-available package at http://www.libradtran.org, "libRadtran" [*Mayer et al.*, 1997] was used for calculations of radiative transfer in the twilight conditions. The software exploits a pseudo-spherical version SDISORT of the well-known DISORT algorithm. The pseudo-spherical algorithm was developed by *Dahlback and Stamnes* [1991], using Chapman functions to take into account the sphericity of the Earth. The software approximates the aerosol phase function by the Heyney-Greenstein phase function, which is characterized by the single scattering albedo and the

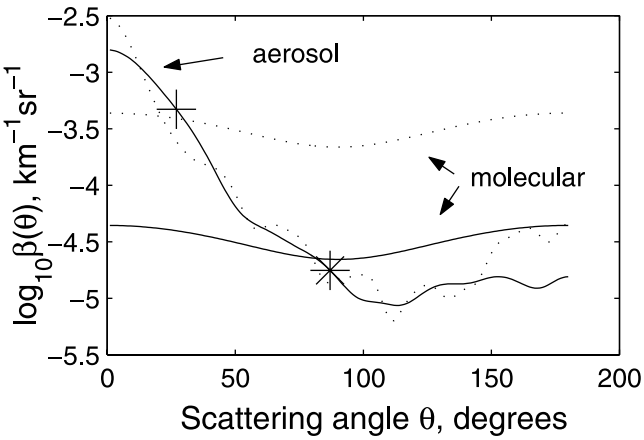

Figure 5. Aerosol and molecular angular scattering $\beta(\theta)$ as a function of light scattering angle θ. Dotted and solid lines correspond to wavelengths 400 nm and 700 nm. Asterisk and cross mark the scattering angle for measurements with viewing zenith angles 0° and 60°. Aerosol extinction was calculated using in situ measurements of post-Pinatubo aerosol size distribution [*Pueschel et al.*, 1994].

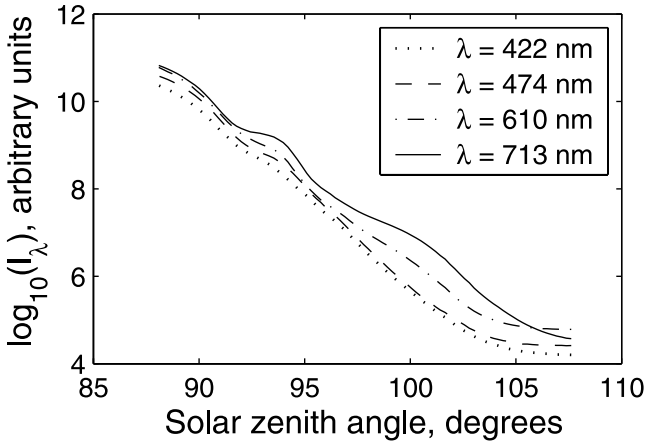

Figure 6. Logarithms of twilight sky brightnesses versus solar zenith angle measured in post-Pinatubo volcanic conditions (November 8, 1991, morning), at different wavelengths. The viewing zenith angle is 60°. The viewing azimuth coincides with the solar azimuth.

asymmetry factor. The δ-M approximation [*Wiscombe*, 1977] is used to accommodate a strongly forward-peaked phase function.

[24] Besides the air density and temperature profiles, the input parameters of the RT model are the ozone profile, the aerosol extinction profile, the single scattering albedo (*SSA*) and the asymmetry factor (*g*), the extraterrestrial spectrum, the Earth's surface albedo, the solar zenith angle, the solar azimuth and the direction of measurements.

[25] The radiative transfer code allows to model twilight sky brightness with acceptable uncertainty of 10% at least up to 93° of SZA for wavelength 340 nm [*Kylling et al.*, 2003]. Unfortunately, we do not have any information about the rise of uncertainty for SZAs larger than 93°. We consider that uncertainties at SZAs larger than 93° are still acceptable until the modeled and the experimental curves will show significant discrepancy. This happens at SZA larger then 95°. This discrepancy is discussed in chapter 5.2.

[26] The following input parameters were used for modeling the twilight sky brightness.

[27] 1. The aerosol extinction profile is the most important parameter, which affects the twilight sky brightness outside the ozone absorption band. In this work we use three types of aerosol extinction profiles. They are: SAGE II [*McCormick*, 1987] aerosol extinction profiles interpolated to the wavelength of measurements, SAGE II aerosol extinction profiles interpolated to the wavelength of measurements and scaled by a factor to fit twilight curves, and modified SAGE II profiles. Here we describe how we obtained the first type of extinction profile, which serves as a basis for the other two. They will be discussed later. We used the monthly averaged SAGE II extinction profiles available at http://www-sage2.larc.nasa.gov for latitude range 40–50°, which contains the latitude of our observational site (41.8°). The logarithm of two SAGE II extinctions adjacent to our measurements were linearly interpolated to the twilight measurements wavelength, hereby implicitly making use of the Ångström law $\tau(\lambda) = \beta_1 \cdot \lambda_1^{-\alpha}$. For low and high altitudes, an extrapolation of the aerosol extinction profile was performed by using the SAGE II 1.02 μm channel. During the period after the Pinatubo eruption, when the saturation of SAGE measurements frequently occurred at low altitudes, a combined profile was used, for which the low altitude extinction was taken from the SAGE II November 1991 profile. In most cases, SAGE profiles do not reach the Earth's surface and the extinction at ground level was assumed to be equal to 0.1 km^{-1}. At altitudes higher than 40 km an exponential decrease of extinction was supposed up to a value of 10^{-9} km^{-1} at 100 km altitude.

[28] 2. The other important parameters are the aerosol single scattering albedo *SSA* and the asymmetry factor *g* parameters. These quantities have to be considered separately for stratospheric and tropospheric aerosols. We suppose in our modeling that the stratospheric aerosol is mostly represented by sulphuric acid droplets which means that its extinction is essentially determined by scattering and SSA is practically equal to 1. This issue is discussed in *Russell et al.* [1996]. The error in the aerosol optical thickness, which is brought by the uncertainty of SSA is discussed in chapter 6.3. The estimates of *g* were made using the EXTRA model of aerosol size distributions [*Fussen and Bingen*, 1999]. A typical value for post-Pinatubo aerosol was $g \approx 0.7–0.75$ for considered range of wavelengths.

[29] 3. For the optical properties of the tropospheric aerosols a global model of aerosol [*D'Almeida et al.*, 1991] was used. The average values for our observational place are $SSA = 0.938$ and $g = 0.67–0.737$. *Kylling et al.* [1998] mentioned a high variability of these parameters, when they tried to fit measured UV irradiances by RT modeling.

[30] 4. The spectral range of observations covers the ozone Chappuis band, with "blue" and "red" channels on the edges of the band, so that changes of ozone column will affect twilight curves for these channels minimally. Ozone is assumed 300 DU and its influence will be considered later.

[31] 5. The azimuth of viewing direction coincides with the azimuth of the Sun.

[32] 6. A value of surface albedo does not have a significant influence on a calculated twilight curve due to the geometry of observations (see Figure 1). It was set to 0.1, which is a characteristic value for vegetation.

[33] 7. The US standard atmosphere was used.

[34] 8. The refraction is especially important in twilight conditions. For example, at SZA = 95° it causes a difference of about 9 km in the calculated altitude of the Earth's shadow.

[35] In twilight curve modeling, we considered SZA's up to 97°. When SZA exceeds this limit the code starts to give obviously wrong results, namely oscillations instead of a monotonous decrease.

5. Structure of the Twilight Sky Brightness

[36] In this section we model the radiative field of the twilight sky for volcanically quiet and volcanically disturbed conditions. For a better understanding of the variations of the twilight sky brightness let us consider the following numerical experiment. We suppose spectral measurements of the zenith sky brightness and assume that an

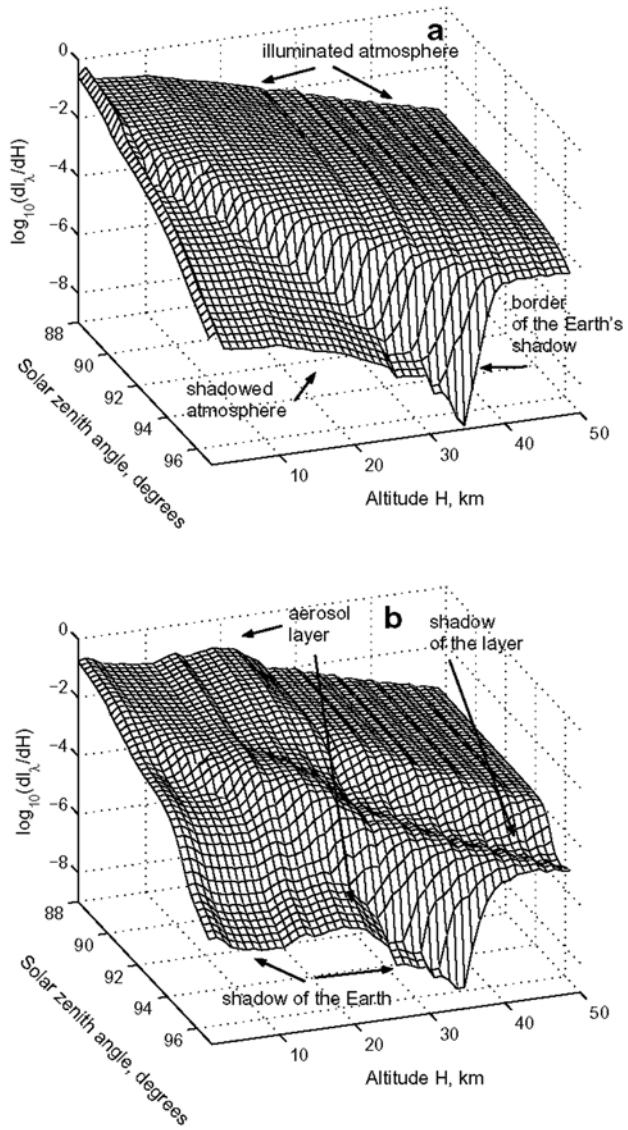

Figure 7. (a) Modeled contributions of scattering volumes with thickness ΔH located at different altitudes H to the intensity of twilight light directed towards the observer for each value of the solar zenith angle. Volcanically quiet aerosol conditions are used in this situation. Ozone content is 300 DU, the wavelength of modeling λ = 700 nm. The monthly and zonal averaged SAGE II aerosol extinction profile attributed to February 1989 and interpolated to the wavelength 700 nm is used for the modeling. (b) The same as in Figure 7a, in volcanic conditions. The monthly and zonal averaged SAGE II aerosol extinction profiles attributed to the November 1991 and interpolated to the wavelength 700 nm is used for the modeling.

observer is located at an altitude H, which varies from 0 to 50 km. Such measurements $I_\lambda(H, SZA)$ are modeled with the aid of the RT code for different values of SZA. As a result we have a set of twilight curves, as if they are measured from different altitudes. The derivative $\partial I_\lambda/\partial H$ for a fixed value of SZA will show a contribution of scattering volumes with thickness ΔH located at different altitudes H to the twilight sky brightness measured from the ground level.

[37] Figure 7 shows a surface $\partial I_\lambda/\partial H(H, SZA)$ in logarithmic scale at 700 nm wavelength for volcanically quiet (a) and volcanically disturbed (b) conditions. Let us consider first volcanically quiet case. A sharp step in the dependence of $\partial I_\lambda/\partial H(H)$ clearly indicates a boundary between sunlit and shadowed parts of the atmosphere. It should be mentioned that in the shadowed part of the atmosphere the sky brightness decreases with H faster than it would be expected from an exponential decrease of atmospheric density. This effect is caused by ozone absorption. Figure 8 shows the dependence $\partial I_\lambda/\partial H(H)$ modeled for average and low ozone content conditions. We can see that in the latter case the dependence becomes indeed more exponential. This effect depends on wavelength and in the Chappuis band the values of $\partial I_\lambda/\partial H(H)$ become negative below the Earth's shadow showing strong absorption.

[38] Let us now consider how an enhanced aerosol layer disturbs the surface $\partial I_\lambda/\partial H(H, SZA)$ (Figure 7b). There is a clear ridge at the altitude of the layer extended along the entire considered range of SZA. The ridge crosses the Earth's shadow and is located partly in sunlit, partly in shadowed atmosphere. The light attenuation in the aerosol layer causes a deep valley that intersects the layer and then runs in parallel to the boundary of the Earth's shadow. It is indicated on Figure 1 by a grey band. An increase of the intensity between the shadow of the layer and shadow of the Earth, causes a hump on the twilight curves. In case of a dense and broad aerosol layer we should expect that the attenuation in the layer will depress the enhancement of intensity due to the scattering and we will see only a grey shadow instead of spectacular twilight colors. *Stothers* [1996] showed that when the vertical optical thickness of SAL (after a large eruption) exceeds 0.15, twilight glow disappears. After the eruption of Katmai (6 June 1912), the twilight glow disappeared between mid-June and late September [*Volz*, 1975]. Following the Tambora eruption in 1815, twilight glows were suppressed for a very long time, between late September 1815 and July 1818 [*Stothers*, 1996].

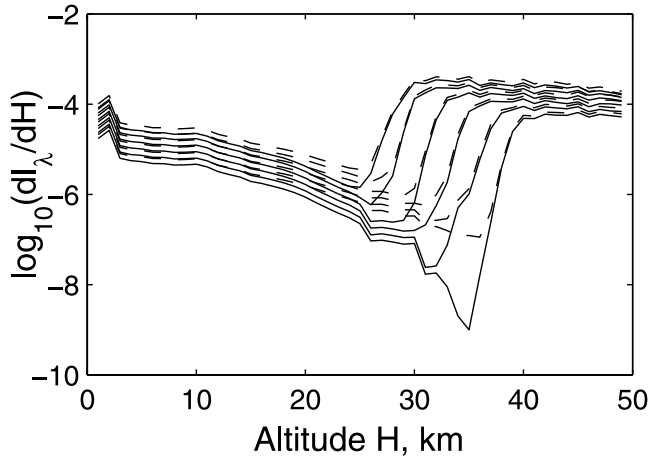

Figure 8. The same as on Figure 7a for solar zenith angle range 95.8–96.8° modeled for conditions of average (300 DU, solid line) and low (50DU, dashed line) ozone content, λ = 700 nm.

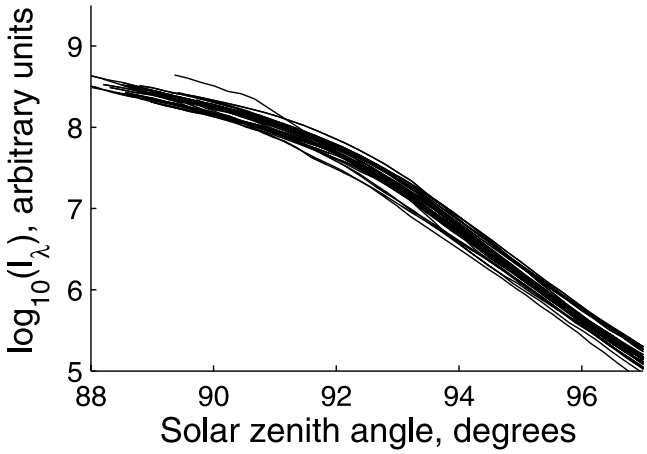

Figure 9. Logarithms of twilight sky brightnesses versus solar zenith angle (February–October 1989) measured in volcanically quiet conditions for λ = 713 nm. The viewing zenith angle is 0°. Annual variations are clearly visible.

[39] The modeling shows that in case of an enhanced SAL the light scattered by the SAL may be more intensive than the light scattered by tropospheric aerosol even if the Sun is slightly above the horizon. In chapter 7 we discuss discrepancies between the experiment and the theoretical analysis presented above.

6. Twilight Sky Brightness at Moderate SZA

[40] In this section we consider the experimental results and try to get quantitative characteristics of the stratospheric aerosols with the help of RT modeling. We restrict our consideration SZA's less then 97° due to limitations of the RT code.

6.1. Twilight Sky Brightness in Volcanically Quiet and Volcanically Disturbed Conditions

[41] Here we try to fit experimental twilight curves by modeled ones for volcanically quiet and volcanically disturbed conditions and investigate the influence of tropospheric aerosol variations on twilight sky brightness. We should emphasize that the absence of absolute calibration of the experimental twilight sky brightness did not allow us to consider spectral variations of twilight sky brightness and forced us to use each channel data separately for the aerosol extinction retrieval.

[42] Figure 9 shows twilight curves measured in 1989 at 713 nm. The curves show some variability. To understand a possible reason for the variation, twilight curves were computed using SAGE II aerosol extinction profiles related to the appropriate months and latitudinal belt, which were interpolated to the wavelength of measurements. The theoretical curves also show the same variability as the experimental ones. Subsequent modeling showed that the variations are driven by the tropospheric aerosol fluctuations. When the tropospheric aerosol is sunlit it contributes to the scattered light and as soon as it enters the Earth's shadow, it continues to attenuate light scattered by higher and still sunlit layers of the atmosphere.

[43] Before attempting to fit particular measurements by modeled twilight curves we should mention that the measurements are expressed in arbitrary units. It means that we can compare only shapes of the theoretical and experimental curves, not their absolute values. For this comparison exercise, the modeled curves were shifted in logarithmic scale up to coincidence with experimental ones at SZA = 90°. This value of SZA was chosen for the following reasons. For smaller SZA, a better quality of the pseudo-spherical approximation is expected as well as a better signal-to-noise ratio. On the other hand, when the Sun is above the horizon some direct sun rays may be scattered into the photometer.

[44] To fit the experimental twilight curves attributed to the volcanically-quiet period, monthly averaged SAGE II profiles for the latitudinal belt 40–50° were used. SAGE II aerosol extinction profiles (for the months corresponding to those of measurements) were interpolated to the wavelength of one channel of the twilight photometer centered at 713 nm. The profile was scaled by a factor. Then a best fit profile was searched by varying the scaling factor and calculating the mean square deviation between the modeled and the experimental twilight curves. Figure 10 shows an example of such fitting. The discrepancy at SZA greater than 95° will be discussed later.

[45] For measurements attributed to the volcanically-disturbed period, the simple scaling of SAGE II extinction profiles does not give a satisfactory agreement with the experiment. The modified SAGE II profiles are required. The following procedure was used. The aerosol extinction profile was considered as a combination of a "basic" profile and a "stratospheric layer". The SAGE II profiles were cut in such a way that only two segments -lower tropospheric one and stratospheric segment located above the aerosol layer were saved. The gap between the two segments was filled up with a straight segment. In such a way we obtained the aerosol extinction profile without the stratospheric aerosol layer (mentioned as a "basic" profile). The two SAGE II profiles (interpolated to the wavelength of twilight

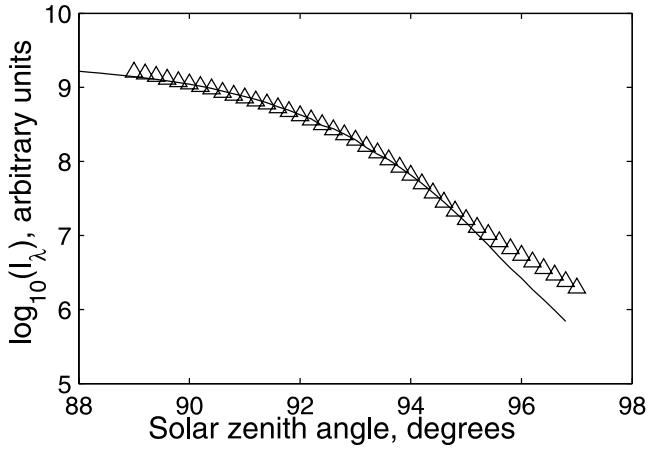

Figure 10. An example of a twilight curve (logarithms of twilight sky brightnesses versus solar zenith angle) measured in volcanically quiet conditions in February 5, 1989, morning (triangles) and a fitting modeled curve (solid line). The wavelength of measurements is 713 nm. The viewing zenith angle is 60°. The viewing azimuth coincides with the solar azimuth.

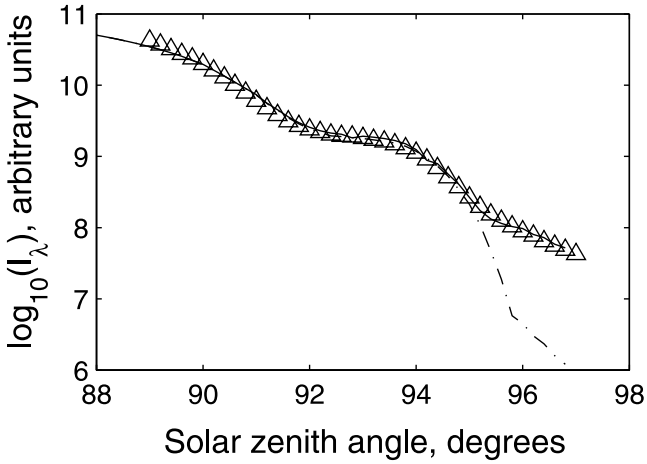

Figure 11. An example of a twilight curve (logarithms of twilight sky brightnesses versus solar zenith angle) measured in volcanically disturbed conditions in November 8, 1991, morning (triangles). Two fitting modeled curves are: dash-dotted line is calculated using the aerosol extinction profile which is presented on Figure 5 (solid line); solid line is calculated using the same profile with added mesospheric aerosol layer (Figure 5, dotted line). The wavelength of measurements is 713 nm. The viewing zenith angle is 60°. The viewing azimuth coincides with the solar azimuth.

measurements as it is described above) for February 1989 and November 1991 were used to prepare the "basic" profiles. The February 1989 profile was used for modeling all twilight measurements of August–September 1991 and of August–November 1993. For the rest of the twilight measurements a SAGE profile for November 1991 was used. Then the stratospheric aerosol layer was modeled by a parabola, which was added to the "basic" profile prepared as it is described above.

[46] The parabola was determined by the following input parameters: magnitude, half-width and altitude of maximum. The combined profiles were calculated according to the RT code format. Look-up tables were computed and the best-fit profile was sought by a least-squares. An example of a fitted curve is presented in Figure 11. We can see again a good agreement between the theory and measurements up to 95°.

6.2. Aerosol Optical Thicknesses and Aerosol Extinction Profiles

[47] Here we consider aerosol optical thicknesses and aerosol extinction profiles obtained from twilight measurements. The annual variations of the optical thicknesses obtained from both twilight measurements and SAGE II were considered. The twilight and SAGE II extinction profiles were integrated from 10 to 30 km. The twilight measurements in the channel centered at 713 nm were chosen. This choice was made to minimize a contribution of the Rayleigh scattering by air molecules and, thus, to enhance aerosol effects. We have not used the 810 nm channel because the modeling of twilight curves is complicated by the presence of water vapor absorption lines in this spectral region.

[48] Figure 12 shows the temporal evolution of the optical thickness. There is a good agreement between SAGE II and twilight results. The considered time interval (1990–1993) includes the Pinatubo eruption in June 1991. The SAL starts to grow already in August 1991, then reaches its maximum at the end of 1991-beginning of 1992 and decays slowly till the end of 1993, still exceeding the pre-Pinatubo background level. We should mention that we can not expect a full agreement between SAGE II data averaged monthly and over the latitudinal belt 40° to 50°, and twilight data, which were obtained in a particular day (in morning or evening) and from a particular observational site. For the same reason we should expect that the twilight data would show more variability. We should also take into account that SAGE II data were saturated below about 14 km in 1992. We extrapolated them down to about 10 km, as it was described in chapter 4, when we integrated SAGE II extinctions for obtaining optical thicknesses (Figure 12). One more reason for the discrepancy in 1992 could be the eruption of Mount Spurr (Alaska) in August 18, 1992 [*Smithsonian Institution*, 1992]. This might cause a non-homogenous distribution of aerosol between eastern and western hemispheres within the 40–50° latitudinal belt and enhanced SAGE II optical thickness in comparison with the twilight data, which were obtained in the eastern hemisphere. We also should mention a possible patchy structure of the stratospheric aerosol cloud. *Antuña et al.* [2003] analyzed variability of the Pinatubo aerosol cloud using SAGE II profiles consecutive in time and space. They have found a variability 20–40% for a time lapse of 12 hours and 50–150% for time lapses of 24 and 48 hours in the tropics for the period of six months after the eruption.

[49] The spectral dependence of the aerosol extinction is completely different for pre-Pinatubo and post-Pinatubo measurements. Figure 13 depicts the spectral dependence of aerosol extinction at 20 km in case of background conditions as obtained from the twilight measurements and SAGE II experiment. In general, both dependences

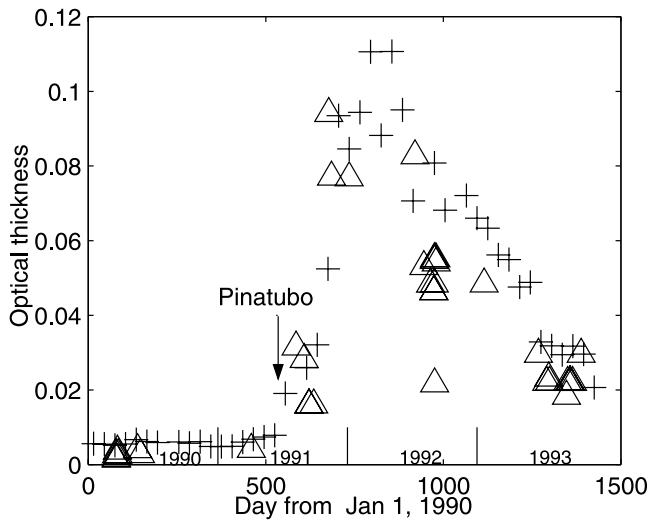

Figure 12. Temporal evolution of the optical thickness obtained from SAGE II (crosses) and twilight measurements (triangles). The wavelength of measurements is 713 nm. The SAGE II data are interpolated to the same wavelength.

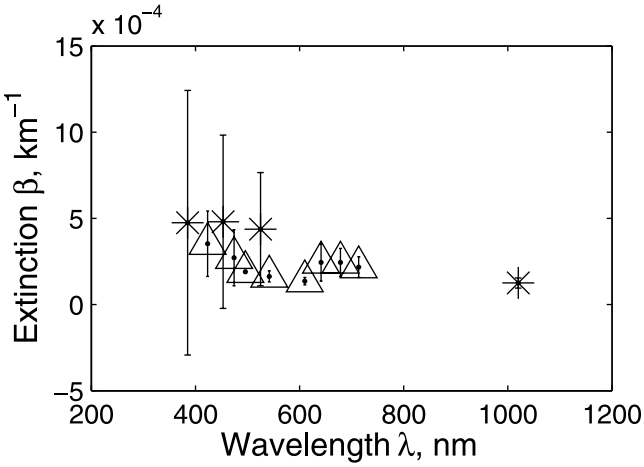

Figure 13. Spectral dependence of the aerosol extinction at 20 km altitude volcanically quiet conditions obtained from SAGE II (February 1989, asterisks) and twilight measurements (February 5, 1989, morning, triangles).

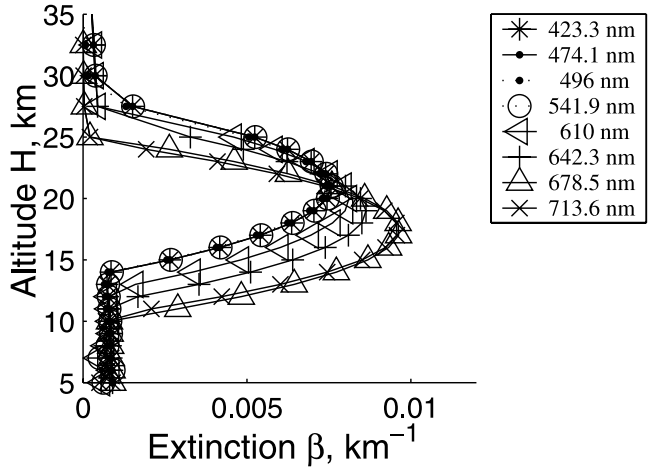

Figure 14. Aerosol extinction profiles for volcanically disturbed conditions (November 8, 1991, morning), at different wavelengths, obtained from twilight measurements.

exhibit the same behavior: the extinction decreases with increasing wavelengths. According to Mie theory this kind of dependence is characteristic for small aerosol particles with effective radius $r \sim 0.2$ μm.

[50] Figure 14 depicts the spectral dependence of the aerosol extinction profiles obtained from twilight measurements in volcanically disturbed conditions, namely in Nov. 1991. These profiles are characterized by an increase of the SAL component with increasing wavelengths and a decrease of the altitude of the profile maximum. To understand these features, we can consider the spectral dependence of the extinction profiles at different altitudes (Figure 15). We see that the extinction maximum shifts towards longer wavelength with the decrease of altitude. According to Mie theory such shift is connected with an increase of the effective radius of aerosol droplets. It means that the larger aerosol droplets accumulate at lower altitude and the effective radius of the aerosol decreases with altitude. So, according to our data the effective radius must increase with the decrease of altitude to at least as low as 17 km. This fact is in full agreement with *Anderson and Saxena* [1996]. They obtained the same vertical dependence of the aerosol effective radius by analyzing the SAGE II extinction profiles and have shown that the value of the effective radius reaches maximum even lower, at about 15.5 km altitude.

[51] *Berthet et al.* [2002] measured stratospheric aerosol extinction by balloonborne spectrometers. The two balloonborne measurements performed at the dates when the atmosphere was still affected by the Pinatubo eruption, in October 1993 and March 1994, also show altitudinal variations of the wavelength dependences similar the twilight data had. Namely, the extinction maximum shifts towards longer wavelength with the decrease of altitude. The balloonborne measurements attributed to the volcanically quiet period, February 2000, show the same type of wavelength dependence as presented on Figure 13, the decrease of extinction towards longer wavelengths.

[52] Here we should remember that while obtaining extinction profiles for different wavelengths we supposed an ozone column of 300 DU. But some of the channels are centered within the ozone Chappuis band and the actual ozone column may turn out to be important for a correct modeling. Twilight curves modeled for different ozone contents and shifted in logarithmic scale for coincidence with the experimental one are almost similar by shape. We conclude that we can neglect the ozone influence when comparing experimental and modeled curves by shape. This feature is important because it simplifies the inversion procedure. The error, which is brought in with an uncertainty of ozone column, is discussed in chapter 6.3.

6.3. Expected Uncertainty of the Optical Thickness

[53] Here we present a rough estimate of the uncertainty for one of the spectral channels of our measurements (713 nm) for high aerosol loading, such as that after the Pinatubo eruption. We should take into account a number of uncertainty sources, which influence a finally retrieved value of the optical thickness. They are a measurement error, forward model errors, modeling parameter errors and an error caused

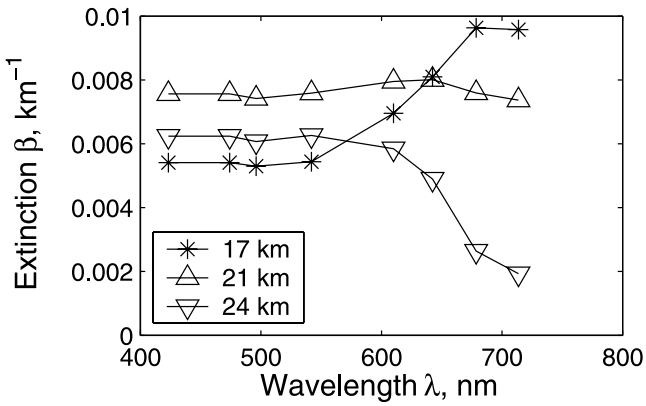

Figure 15. Spectral dependences of the aerosol extinction at different altitudes for volcanic conditions (November 8, 1991, morning) obtained from twilight measurements.

by using look up tables with a finite step of variable parameters of the stratospheric layer.

[54] Some errors depend on the wavelength of measurement and the value of the stratospheric aerosol optical thickness. Namely, Rayleigh scattering increases dramatically with the decrease of the wavelength of measurement and variations in atmospheric properties become more important, especially at low values of the stratospheric aerosol optical thickness.

[55] The measurement error did not exceed 1% and other sources of error contributed more into the overall uncertainty. We made a rough estimation of uncertainties caused by input modeling parameters in the following way. We considered modeled twilight brightnesses with input parameters differing only by magnitude (with step of value Δm) of the stratospheric aerosol layer. The mean square deviations (Δf) of the modeled twilight brightness curves in the range 89°–94° of SZA were estimated. Then we estimated mean square deviations of modeled twilight brightness curves caused by the uncertainty of each input parameter. We converted the mean square deviations into the error of the magnitude of the layer by multiplying them by a factor $\Delta m/\Delta f$. With the aid of this procedure we have analyzed the errors listed above.

[56] First, the following forward model errors were analyzed. The difference in the modeled twilight curves caused by a possible variation of atmospheric parameters, was estimated. The deviation caused by using summer and winter midlatitude models of the atmosphere instead of the US standard atmosphere brings an uncertainty of about 1%.

[57] *Kylling et al.* [2003] compared the modeled UV irradiances and balloon-based measurements. For the wavelength 340 nm the simulations and measurements agreed within 10% up to SZA 93°. Our estimate of the corresponding error of the layer magnitude is also 10%.

[58] Then, the variations of stratospheric aerosol parameters such as single scattering albedo (we varied it in the range $0.9 \div 1$) and asymmetry factor ($g = 0.75 \pm 0.05$) lead to an uncertainty of 2% and 3% respectively.

[59] Differences in a priori values of lower tropospheric and stratospheric (above the stratospheric layer) extinctions, such as that between the two SAGE II profiles of February 1991 and November 1991 used for preparing the "basic" profiles, bring 11% error.

[60] The modeling parameter errors consist of the instrument error and the error, which is brought in by contaminant species (ozone in our case). We consider the instrument errors caused by the uncertainties (±0.25°) in zenith angle and azimuth of photometer pointing, and also by filter halfwidth (5 nm). The instrument errors induce an uncertainty of about 2.5%. Uncertainties induced by ozone were considered for the 610 nm wavelength. Ozone variations (300 ± 50 DU) lead to 3% uncertainty. We should keep in mind that we consider the influence of ozone changes on the shape of twilight curves, not on their absolute values.

[61] The used steps of look up tables for altitude and halfwidth of the stratospheric layer were 0.5 km, leading to uncertainties in the altitude and halfwidth 1.5% and 2.5% respectively.

[62] The previous discussion allows us to conclude that a reasonable estimate of the uncertainties of stratospheric aerosol optical thickness presented in this paper is 20–30% in case of high stratospheric aerosol loading, such as that after the Pinatubo eruption. The accuracy may be significantly improved by a better choice of a priori parameters, which cause the bulk of the uncertainty.

[63] We should also mention that the simple parabolic approximation of the stratospheric aerosol layer used here was not always valid. In some cases the layer seemed definitely asymmetric. For example the fitting error for the measurements soon after the Pinatubo eruption (namely, in August 1991) was much higher and exceeded 100%. An approximation by an asymmetric shape should decrease this error to a reasonable value.

7. Twilight Light Brightness at Large SZA

[64] In this section we discuss a possible origin of humps II (Figure 2) and the discrepancy between the theory and experiment at SZAs greater than 95°. The modeled twilight curves show a tendency to slope down steeper than the experimental ones at SZAs greater than 95° degrees (Figure 11). This tendency grows with the increase of stratospheric aerosol loading (compare, for example, Figures 10 and 11). The behavior of the modeled curve may be understood by inspecting Figure 1. The SAL casts a shadow on the upper layers of the stratosphere and they do not contribute to the light scattered towards the observer.

[65] We consider the following hypotheses of the origin of the hump II and of the discrepancy between the modeling and experiment. This discrepancy may be caused by (1) the single scattering on mesospheric aerosol and (2) the secondary scattering by the stratospheric aerosol layer.

[66] First let us discuss a possibility of single scattering in the mesosphere to be a reason of the hump II. Figure 11 shows that an aerosol extinction profile with a mesospheric aerosol layer (presented on Figure 4 by dotted line) is able to fit the experimental twilight curve exactly. The mesospheric aerosol extinction required for fitting the experimental curve by the model appeared to be about 2×10^{-5} km^{-1} at 80 km. This value is slightly larger than the extinction coefficient 6.1×10^{-6} km^{-1} obtained for polar mesospheric clouds [*Debrestian et al.*, 1997]. We can hypothesize a presence of an enhanced aerosol layer in the mesosphere as a consequence of a deep penetration of the volcanic gases in the mesosphere. Very small sulfuric acid aerosol droplets might also be lifted to the mesosphere by upwelling processes in the tropical atmosphere. But this hypothesis faces serious difficulties. *Rinsland et al.* [1995] reported an observed increase of SO_2 mixing ratio at about 50 km altitude. They made a conclusion that a possible source of SO_2 may be the photolysis of H_2SO_4. *Vaida et al.* [2003] suggested that at high altitudes exitation of vibrational overtones of H_2SO_4 and its hydrate in the near-infraread and visible leads to photolysis, forming SO_3 and water. *Reiner and Arnold* [1997] pointed out that the reaction of recycling of H_2SO_4 from SO_3 is too slow at altitudes above 40 km. They concluded that a result of the suppression of H_2SO_4 formation above 35–40 km is that aerosols cannot be composed of liquid H_2SO_4/H_2O droplets since the measured H_2SO_4 vapor pressure is much lower than the equilibrium saturation pressure.

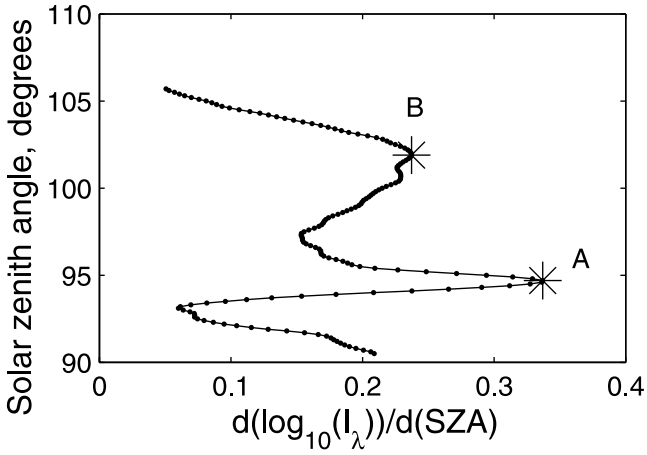

Figure 16. The derivative of the post-Pinatubo twilight curve presented on Figure 6. The wavelength of measurements is λ = 713 nm. Points A and B correspond to the points of the maximal rates of decay marked with asterisk and cross in Figure 2.

[67] These objections lead us to the preference of the secondary scattering by SAL hypothesis over the single scattering on mesospheric aerosol. We cannot also suppose that hump II is caused by mesospheric aerosol of meteoric origin because the hump II does not occur in twilight curves obtained during the volcanically quiet period and is a persistent feature of twilight curves obtained after the Pinatubo eruption.

[68] We guess that the most likely origin of the hump II is secondary scattering in the SAL. The following reason might prevent the used RT code to model this secondary scattering. In the "pseudo-spherical" approximation the direct beam attenuation is computed correctly using the spherical geometry (i.e. Chapman function). The multiple scattering is included using the plain-parallel approach [*Dahlback and Stamnes*, 1991]. We should conclude that if the multiple scattering causes the hump II it is very likely that the RT code is not able to simulate it.

[69] Figure 1 illustrates how "hump I" may be a source of light for "hump II". The light scattered by "hump I" towards the night part of the atmosphere is bounded by the surface of the Earth from one side and by the SAL from the other side. The SAL strongly attenuates tangent rays, so only the light traveling beneath it through the troposphere can be scattered by a farther segment of the SAL towards the observer. Practically the explanation of the hump II phenomenon is analogous to the explanation of the hump I. We should expect that hump II as well as hump I would be more prominent in longer wavelengths, because in this case the light penetrates the troposphere easier. Figure 6 shows a spectral variation of the experimental twilight curves and, indeed, hump II practically vanishes at short wavelengths. Figure 14 shows that aerosol extinction increases with wavelength in post-Pinatubo conditions. In such a case single scattering may also be more efficient at longer wavelengths causing more prominent humps.

[70] If we accept hump I as a light source for hump II we should expect a correlation between the SZA = $\alpha + \pi/2$ (α is the angle AOC) at which hump I decays and the SZA = $\beta + \pi/2$ (β is the angle AOE) at which hump II decays (Figure 1). The corresponding points are marked with asterisk and cross in Figure 2. The relationship between α and β must be linear in first approach according to a simple geometry (Figure 1). Let us consider the sun ray SC_1 which is tangent to the Earth's surface in point A and is scattered by the SAL in point C_1. The ray C_1E represents a part of the scattered light that is able to reach the further segment of the SAL (see the description above). The ray is tangent to the Earth's surface in the point D. This means that the triangles AOC_1 C_1OD and DOE are right triangles. Their sides OA and OD are equal to the Earth's radius, and the sides OC_1 and OE are equal to the Earth's radius plus the altitude of the SAL. So, in the three triangles AOC_1, C_1OD and DOE we have three equal elements and hence these triangle are equal themselves. As a consequence the angles AOC_1, C_1OD and DOE are equal, so $\beta = 3\alpha$. Figure 16 shows a derivative of the logarithm of the twilight curve for one of the post-Pinatubo observations. Letters A and B mark maxima of the derivative and correspond to points C_1 and E in Figure 1 and to points marked by asterisk and cross in Figure 2. Figure 17 shows correlation between solar depression angles of points A and B for observations in the 1991–1993 period. The correlation coefficient is 0.56, a significant value. The mean relationship β/α is 2.5 ± 0.3 close to the expected value of 3.

[71] We should conclude that the secondary scattering in the SAL might be a reason of significant increase of twilight sky brightness at large SZA. Turning back to the structure of twilight sky brightness discussed in chapter 5, we should mention that the measurements bring the following correction to the theoretical model of the radiative field of the twilight sky in volcanically disturbed conditions (Figure 7b). We see on Figure 7b that the SAL causes a ridge of light enhancement located partly in the sunlit, partly in the shadowed atmosphere. The experiment shows that the part of this ridge, which extends into the shadow must be more prominent than the modeling gives. We see that after a strong volcanic eruption the radiative field of the atmosphere is significantly disturbed. This should be taken into

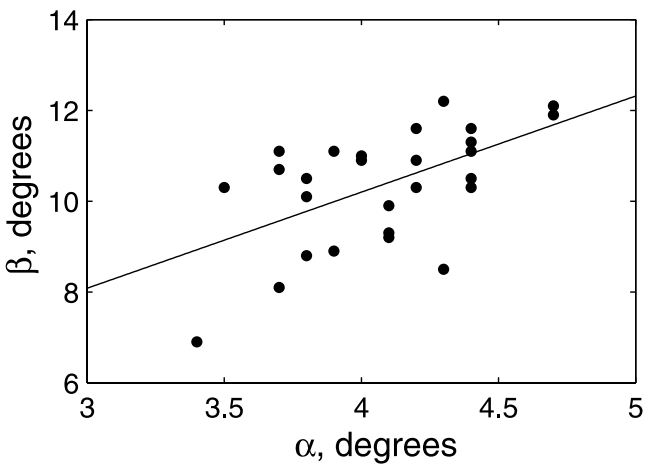

Figure 17. Correlation plot for hump I and hump II. α and β are equal to the solar zenith angles of the points A and B (Figure 16) with 90° extracted. The correlation coefficient is 0.56. The solid line indicates the linear trend.

account in photochemical models using photodissociation rates for different atmospheric species.

8. Conclusions

[72] In this paper we present spectral photometric measurements of the twilight sky brightness and show how such measurements can provide quantitative information about the parameters of the stratospheric aerosol layer. For this purpose we analyze the measurements of twilight sky brightness, which cover the period 1989–1994 including the Pinatubo eruption in June 1991. The enhancement of stratospheric aerosol after the eruption caused a significant disturbance of the twilight sky radiative field. The ''humps'' appeared on the dependences of twilight sky brightness versus solar zenith angle (twilight curves). The hump I occurred in the range of SZA's 92–94° and a less prominent hump II in the range 98–100°.

[73] The pseudo-spherical radiative transfer code ''libRadtran'' was used to analyze these features. The modeled curves reproduced hump I but failed to reproduce hump II. The modeling showed that the hump I was clearly connected to the extinction and primary scattering in the stratospheric aerosol layer. The simple geometric assumptions about light propagation allowed us to suggest that the humps II were likely caused by secondary scattering in the SAL.

[74] The modeling has shown that the shape of twilight curves is quite sensitive to the input aerosol extinction profile. Fitting the twilight curves by modeled ones, we could obtain aerosol extinction profiles for each twilight curve. Due to limitations of the RT code we considered only humps I in our fitting procedure. With the aid of a full spherical radiative transfer code the humps II might also be utilized to extract stratospheric aerosol parameters as well as humps I.

[75] The procedure of fitting was different for curves attributed to volcanically quiet and volcanically disturbed periods. For the volcanically quiet period the extinction profiles where obtained by scaling SAGE II profiles, monthly averaged and interpolated to one of the wavelength of twilight measurements. For the volcanically disturbed period the SAL was modeled by a parabola which was added to the ''basic'' profiles. The parameters of the parabola such as magnitude, altitude and halfwidth of maximum were subject to fitting. In most cases this ''parabolic'' approximation allowed us to achieve a good agreement between the experimental and modeled twilight curve.

[76] The modeling shows that ozone does not significantly influence the shape of the twilight curves, only the magnitude, so it is easy to separate aerosol and ozone contributions to the light intensity.

[77] The optical thicknesses of the SAL where estimated by integrating the fitted aerosol extinction profiles. We considered the spectral channel of the twilight photometer centered at 713 nm. The monthly averaged SAGE II extinction profiles were interpolated to the wavelength of twilight measurements and also integrated. Optical thicknesses of the SAL obtained from the twilight measurements in the 1990–1993 period which includes the Pinatubo eruption, show a good agreement with SAGE II results.

[78] The aerosol extinction profiles obtained by means of fitting measurements of different spectral channels by modeled twilight curves were used to derive spectral dependences of stratospheric aerosol extinction for pre-Pinatubo and post-Pinatubo measurements. These dependences reflect aerosol growth after the eruption.

[79] The obtained results show that twilight measurements might serve, together with other ground-based techniques such us lidar measurements of aerosol backscatter coefficient and sunphotometer measurements of total stratospheric and tropospheric aerosol optical thickness, to validate satellite measurements of stratospheric aerosol. The advantage of twilight measurements is that it can clearly distinguish between the tropospheric and stratospheric optical thicknesses because the troposphere occurs in the Earth's shadow while the stratosphere is still sunlit during twilight. Moreover, it is possible to retrieve aerosol extinction profiles from the twilight measurements. We suppose that the twilight measurements could give especially good results in combination with lidar measurements because lidars give better vertical resolution and twilight measurements give a spectral dependence of aerosol extinction which is important for the subsequent retrieval of aerosol size distribution. We should also stress that twilight measurements allow an easy separation of aerosol and ozone optical thicknesses.

[80] **Acknowledgment.** N. Mateshvili was supported by grant ''Coopération S&T avec l'Europe centrale et orientale'' of the BELSPO Service of the Belgian Government.

References

Ackerman, M., et al. (1989), European validation of SAGE II aerosol profiles, *J. Geophys. Res.*, *94*, 8399–8411.

Anderson, D. E., R. Demajistre, S. A. Lloyd, and P. K. Swaminathan (1995), Impact of aerosols and clouds on the troposphere and stratosphere radiation field with application to twilight photochemistry at 20 km, *J. Geophys. Res.*, *100*, 7135–7146.

Anderson, J., and V. K. Saxena (1996), Temporal changes of Mount Pinatubo aerosol characteristics over northern midlatitudes derived from SAGE II extinction measurements, *J. Geophys. Res.*, *101*, 19,455–19,463.

Antuña, J. C., A. Robock, G. Stenchikov, J. Zhou, C. David, J. Barnes, and L. Thomason (2003), Spatial and temporal variability of the stratospheric aerosol cloud produced by the 1991 Mount Pinatubo eruption, *J. Geophys. Res.*, *108*(D20), 4624, doi:10.1029/2003JD003722.

Ashok, N. M., H. C. Bhatt, T. Chandrasekhar, and J. N. Desai (1982), Twilight IR brightening over India due to EL Chichon's eruption in Mexico, *Nature*, *300*, 620–621.

Ashok, N. M., H. C. Bhatt, T. Chandrasekhar, J. N. Desai, and D. B. Vaidya (1984), Twilight optical studies of the El Chichon volcanic dust over Ahmedabad, India, *J. Atmos. Terr. Phys.*, *46*, 411–418.

Berthet, G., J.-B. Renard, C. Brogniez, C. Robert, M. Chartier, and M. Pirre (2002), Optical and physical properties of stratospheric aerosols from balloon measurements in the visible and near-infrared domains. I. Analysis of aerosol extinction spectra from the AMON and SALOMON balloonborne spectrometers, *Appl. Opt.*, *41*, 7522–7539.

Chakrabarty, D. K., and M. Lal (1997), Spectroscopic study of twilight intensity in the red region over Ahmedabad (23°N) after the Mt. Pinatubo eruption, *J. Atmos. Terr. Phys.*, *59*, 1143–1148.

Dahlback, A., and K. Stamnes (1991), A new spherical model for computing the radiation field available for photolysis and heating at twilight, *Planet. Space Sci.*, *39*, 671–683.

D'Almeida, G. A., P. Koepke, and E. P. Shettle (1991), *Atmospheric Aerosols: Global Climatology and Radiative Characteristics*, 561 pp., A. Deepak, Hampton, Va.

Deacon, E. L. (1956), The second purple light, *Nature*, *178*, 688.

Debrestian, D. J., J. D. Lumpe, E. P. Shettle, R. M. Bevilacqua, J. J. Olivero, J. S. Hornstein, W. Glaccum, D. W. Rusch, C. E. Randall, and M. D. Fromm (1997), An analysis of POAM II solar occultation observations of polar mesospheric clouds in the southern hemisphere, *J. Geophys. Res.*, *102*, 1971–1982.

Fussen, D., and C. Bingen (1999), A volcanism dependent model for the extinction profile of stratospheric aerosols in the UV-visible range, *Geophys. Res. Lett.*, *26*, 703–706.

Gann, U. (1902), *The Earth, Its Atmosphere and Hydrosphere* (in Russian, translation from fifth German edition), 320 pp., Brokgauz i Efron, St. Petersburg, Russia.

Kylling, A., A. F. Bais, M. Blumthaler, J. Schreder, C. S. Zerefos, and E. Kosmidis (1998), Effect of aerosols on solar UV irradiances during the Photochemical Activity and Solar Ultraviolet Radiation Campaign, *J. Geophys. Res.*, *103*, 26,051–26,060.

Kylling, A., T. Danielsen, M. Blumthaler, J. Schreder, and B. Johnsen (2003), Twilight tropospheric and stratospheric photodissociation rates derived from balloon borne radiation measurements, *Atmos. Chem. Phys.*, *3*, 377–385.

Mateshvili, I., G. Mateshvili, and N. Mateshvili (1998), Measurement of the vertical aerosol distribution in the middle atmosphere by the twilight sounding method, *J. Aerosol Sci.*, *29*, 1189–1198.

Mateshvili, N., and F. J. M. Rietmeijer (2002), Stratospheric dust loading from early 1981 to September 1985 based on the twilight sounding method and stratospheric dust collection, *J. Volcanol. Geotherm. Res.*, *120*, 55–69.

Mayer, B., G. Seckmeyer, and A. Kylling (1997), Systematic long-term comparison of spectral UV measurements and UVSPEC modeling results, *J. Geophys. Res.*, *102*, 8755–8768.

McCormick, M. P. (1987), SAGE II: An overview, *Adv. Space Res.*, *7*, 219–226.

Montenbruck, O., and T. Peleger (2000), *Astronomy on the Personal Computer*, 310 pp., Springer, New York.

Pueschel, R. F., P. B. Russell, D. A. Allen, G. V. Ferry, K. G. Snetsinger, J. M. Livingston, and S. Verma (1994), Physical and optical properties of the Pinatubo aerosol: Aircraft observations with impactors and a Sun-tracking photometer, *J. Geophys. Res.*, *99*, 12,915–12,922.

Reiner, T., and F. Arnold (1997), Stratospheric SO_3 upper limits inferred from ion composition measurements: Implications for H_2SO_4 and aerosol formation, *Geophys. Res. Lett.*, *24*, 1751–1754.

Rinsland, C. P., M. R. Gunson, M. K. W. Ko, D. W. Weisenstein, R. Zander, M. C. Abrams, A. Goldman, N. D. Sze, and G. K. Yue (1995), H_2SO_4 photolysis: A source of sulfur dioxide in the upper stratosphere, *Geophys. Res. Lett.*, *22*, 1109–1112.

Rozenberg, G. V. (1966), *Twilight*, 380 pp., Springer, New York.

Russell, P. B., et al. (1996), Global to microscale evolution of the Pinatubo volcanic aerosol derived from diverse measurements and analyses, *J. Geophys. Res.*, *101*, 18,745.

Shakh, G. M. (1969), Enhanced twilight glow caused by the volcanic eruption on Bali island in March and September 1963, *Tellus*, *21*, 636–640.

Smithsonian Institution (1992), *Bull. Global Volcanism Network*, *17*, 8.

Stothers, R. (1996), Major optical depth perturbations to the stratosphere from volcanic eruptions: Pyrheliometric period, 1881–1960, *J. Geophys. Res.*, *101*, 3901–3920.

Vaida, V., H. G. Kjaergaard, P. E. Hintze, and D. J. Donaldson (2003), Photolysis of sulfuric acid vapor by visible solar radiation, *Science*, *299*, 1566–1568.

Volz, F. (1975), Volcanic twilights from Fuego eruption, *Science*, *4196*, 48–50.

Volz, F., and R. Goody (1962), The intensity of the twilight and upper atmospheric dust, *J. Atmos. Sci.*, *19*, 385–406.

Wiscombe, W. J. (1977), The delta-M method: Rapid yet accurate radiative flux calculations for strongly asymmetric phase functions, *J. Atmos. Sci.*, *34*, 1408–1422.

C. Bingen, D. Fussen, and F. Vanhellemont, Belgian Institute for Space Aeronomy, B1180 Brussels, Belgium. (didier.fussen@oma.be)

E. Kyrölä, Finnish Meteorological Institute, Helsinki, Finland.

G. Mateshvili, I. Mateshvili, and N. Mateshvili, Abastumani Astrophysical Observatory, 0160 Tbilisi, Georgia, South Caucasus.